Journal of Intelligent Manufacturing (2024) 35:2645–2652
https://doi.org/10.1007/s10845-023-02166-5

Deviation compensation in LPBF series production via statistical predeformation and structural pattern analysis

Philipp Lechner[1] · Christoph Hartmann[1] · Daniel Wolf[2] · Abdelrahman Habiba[1]

Received: 12 October 2022 / Accepted: 13 June 2023 / Published online: 28 June 2023

Abstract
This article proposes two approaches for a tailored geometrical deviation compensation for Laser-Powder-Bed-Fusion production. The deviation compensation is performed by a non-rigid deformation of the manufacturing geometry in each iteration to reduce the geometrical deviations from the target geometry. It is important for geometric compensation approaches to separate deterministic deviations from random scatter, since compensating scatter can result in unstable behaviour. In order to compensate only deterministic deviations two novel approaches for a local estimation of the scatter are successfully introduced and tested using a hybrid model of a series production cycle.

Keywords Selective laser melting · Additive manufacturing · Series production · LPBF · Preforming · Predeformation · Geometrical deviation compensation

Introduction

Laser-Powder-Bed-Fusion processes (LPBF) are systematically developed for small and medium volume series production in the last years (Schmidt et al., 2017). An important issue for this development is process stability and the management of geometrical deviations due to, for example, high temperature gradients during production (Bourell et al., 2017), batch to batch deviations and other time dependent influences on the dimensional accuracy of the workpieces. Improvement of geometric and dimensional accuracy of additively manufactured parts was addressed in literature in three different fields: A priori optimization of process parameters, online monitoring, or compensation of form deviations with predeformation of the manufacturing geometry. Cao et al. (2021) used a machine learning technique to train a model based on data from simple geometries to minimize surface roughness and increase dimensional accuracy in LPBF processes. Li et al. (2018) presented a simulative approach to predict residual stresses and distortions in SLM processes, which is utilized to minimize distortion by optimizing production parameters. Luan et al. (2019) proposed a data-driven predictive approach to decouple the effect of various error sources. A compensation framework can then be used to improve the geometric accuracy of the LPBF process by adapting the CAD model. Zhang et al. (2019) proposed a CAD compensation algorithm to improve dimensional accuracy of 3D printed parts in LPBF processes. They proposed a predictive regression model based on deformation of manufactured samples. Inverse transformation can then be applied to the reference CAD model to compensate for geometric deviation. Zongo et al. (2020) predict geometrical deviations of AlSi10Mg components numerically and compare these predictions to experimental results, while Ding et al. (2022) compensate geometric deviations in thin-walled

Philipp Lechner and Christoph Hartmann have contributed equally to this work.

✉ Philipp Lechner
philipp.lechner@utg.de

Christoph Hartmann
christoph.hartmann@utg.de

Daniel Wolf
daniel.wolf@iwb.tum.de

Abdelrahman Habiba
a.habiba@tum.de

[1] Chair of Metal Forming and Casting, Technical University of Munich, Walther-Meissner-Strasse 4, 85748 Garching, Germany

[2] Institute for Machine Tools and Industrial Management, Technical University of Munich, Boltzmannstrasse 15, 85748 Garching, Germany

LPBF-manufactured shell lattice structures with a discrete element method simulation, to capture the dynamic interaction behavior between the powder particles. Vasileska et al. (2022) use layer-wise feedback control to correct deviations of overhang-structures. Amor et al. (2022) predict deviations in LPBF processes based on scale and material concentration effects. Akhavan et al. (2023) use a deep learning approach to control part quality in additive processes by classifying regions of the part as underprinted, normal printed, overprinted or empty. This information is used to adjust the manufacturing parameters of future layers. In addition, a comprehensive review of machine learning methods for the control of additive powder bed processes is given by Zhang and Yan (2022).

Hartmann et al. (2019) utilized a predeformation algorithm based on measurement data of the manufactured components. However, to the best knowledge of the authors, there is no research yet, which specifically addresses issues which arise if a geometrical compensation concept is utilized in series production with high quantities. In particular, the distinction between random scatter in the manufactured geometry and deterministic deviations, which can be reproduced by the process, has not been studied yet. To fill this research gap, this article analyses the influence of a systematic predeformation on the dimensional accuracy of the manufactured components in series production with a focus on the separation of random scatter and deterministic geometrical deviations.

Materials and methods

Components and experimental data

The component which is analysed in this article is already in series production in the automotive industry. Figure 1 shows the component front (left) and back (right). The front is the most important functional area for its use case. Therefore, the presented deviation compensation focuses on this area.

The component is produced with an AlSi10Mg powder and 58 individual components in each job. The geometry of 20 specimens from each built job has been optically digitized for three built jobs. Four of these individual components have been unchanged from job to job, while the manufacturing geometry of 16 specimens has been adjusted in job 2 and 3 to compensate for geometrical deviations using Eq. 1, which is detailed in Sect. 2.2. This experimentally obtained geometrical data may be represented as a vector with one scalar deviation value for each node, which quantifies the deviation in normal direction from the surface of the specimen. This data is utilized to measure the job to job scatter of the process and to determine non-linear compensation behaviour.

Predeformation

The geometry of additively manufactured components is usually described by a triangulated surface mesh. The methodology in this article builds on this structure and systematically compensates geometrical deviations by predeformation of the manufacturing geometry in each node of the mesh by comparing the manufactured workpiece geometry and the target geometry. Both are represented by triangulated surface meshes, which are an approximation of the real geometry. Hartmann et al. (2019) proposed Eq. 1 to calculate the manufacturing geometry $\boldsymbol{m}$ for the next iteration $i+1$:

$$\boldsymbol{m}_{i+1} = \boldsymbol{m}_i - \boldsymbol{\alpha}_{i+1}\boldsymbol{w}_i, \tag{1}$$

where $\boldsymbol{m}$ is a vector which describes the predeformation of the manufactured geometry, which is added to the target geometry. This predeformation is measured in normal direction for each node. $\boldsymbol{w}_i$ is a vector with the deviation of the manufactured workpiece geometry, which is the manufactured specimen of job number i, from the target geometry. $\boldsymbol{\alpha_{i+1}}$ is a constant factor for a global non-rigid predeformation. The calculation of $\boldsymbol{w}_i$ requires an optically determined surface mesh of the manufactured geometry, which is fitted to the target geometry using an iterative closest point algorithm. For each node in the target geometry the distance to the manufactured geometry is determined and used as the nodal deviation in $\boldsymbol{w}_i$. From iteration to iteration the predeformation $\boldsymbol{m}_{i+1}$ is calculated by subtracting the current deviation from the predeformation of the last iteration $\boldsymbol{m}_i$.

Monte-Carlo analysis and non-linear behaviour

For a continuous geometrical compensation in a high-volume series production, it is essential to differentiate between deterministic deviations and random scatter, since scatter that affects the workpiece geometry from job to job cannot be compensated by predeformation. Statistical considerations show that the compensation of random scatter in the manufactured geometry by predeformation of the target geometry leads to an increased scatter for series production. This can be quantified by a Monte Carlo sampling of Eq. 1. In this Monte Carlo analysis, the deviation $\boldsymbol{w}_i$ from target is chosen randomly from the experimental data set with constant target geometry (uncompensated). The experimentally-obtained standard deviation of the process is described by $\boldsymbol{\sigma}^{\text{process}}$ for all M nodes. The Monte Carlo calculation simulated a production cycle of 1000 built jobs with a predeformation according to Eq. 1 and compensation factors α ranging from 0.5 to 1.05. Therefore, the calculation results in the mean standard deviation $\boldsymbol{\sigma}^{\text{compensated}}$ of geometrical deviation of each node within a population of 1000 compensated built jobs. Since unstable behaviour is expected for a compensa-

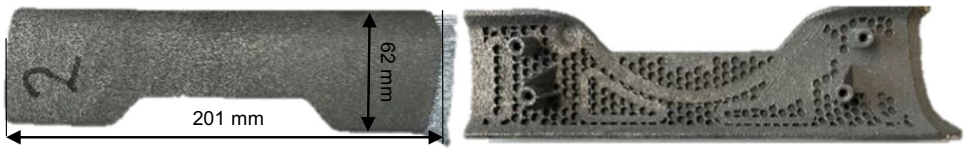

Fig. 1 Specimen of the geometry which serves as an example for LPBF series production in this article

tion factor $\alpha \geq 1$, the calculation is repeated $N = 100$ times for each α to quantify the inherent scatter. To quantify and depict the results, a normalized scatter σ_{norm} is calculated as follows:

$$\sigma^{norm} = \left(\sum_{j=1}^{N} \sum_{k=1}^{M} \frac{\sigma_{jk}^{\text{compensated}}}{\sigma_{jk}^{\text{process}}} \right) / (NM) \tag{2}$$

These considerations assume the compensation process as linear, where a compensation of a node presumes the same reaction in the manufactured geometry. However, recent publications have shown, that this predeformation process is non-linear (Bayerlein, 2020). Therefore, we propose to further develop Eq. 1 by choosing a scaling factor g for each node to cope with the non-linearity of the compensation process, which is highly dependent on the geometry at hand. These considerations lead to Eq. 3:

$$m_{i+1} = m_i - g_{i+1}\alpha_{i+1}w_i \forall \text{ nodes} \tag{3}$$

This equation calculates elementwise the manufacturing geometry for iteration $i+1$. It contains the statistical stability in α_{i+1} and the geometry based inherent non-linearity of the compensation in g_{i+1}.

Separation of scatter and deterministic deviations

In order to reduce the unwanted compensation of scatter, we propose to introduce a third factor p_{i+1}, which is supposed to locally separate scatter from deterministic deviations. This leads to an extended version of Eq. 3:

$$m_{i+1} = m_i - g_{i+1}p_{i+1}\alpha_{i+1}w_i \forall \text{ nodes} \tag{4}$$

In the following, two methods for separating scatter from deterministic deviations are proposed.

The first one uses statistical considerations to design a function p_{stat}, which calculates a factor for each node of the mesh and thus scales the predeformation between 0 and 1, depending on the deviation from target and the typical process scatter at each node. A Gaussian cumulative distribution function, adapted for absolute deviations from target, is utilized to achieve a symmetrical behaviour in Eq. 5:

$$p_{stat}\left(w_i, \sigma_p\right) = \frac{1 + \text{erf}\ |w_i|}{\sqrt{2\left(s\sigma_{process}\right)^2}} - 1 \forall \text{ nodes}, \tag{5}$$

where erf (x) is the Gaussian error function and s is a parameter that determines how significant the deviation has to be compared to the process standard deviation of each node. To calculate p_{stat} the deviations from the target w_i have to be determined analogously to Eq. 1 by fitting the produced geometry to the target geometry. For each node of the target geometry the standard deviation of the experimentally obtained process scatter $\sigma_{process}$ is calculated (as for Eq. 2). Essentially, Eq. 5 weights the absolute value of the geometric deviation from the target against the scatter at that location. If the deviation is small compared to the scatter, the function scales the compensation down. If the deviation is significant compared to the standard deviation of the process, the function converges to 1.

Equation 5 only considers the significance of the deviation for each node compared to the scatter and weights the compensation accordingly. It will be difficult to compensate deterministic deviations that are close to or are smaller than the scatter in absolute terms. Therefore, a second approach is proposed, which is able to compare "deformation patterns". The random scatter in the material and the process conditions leads to specific deformation patterns, which can be categorized into one or multiple deviation classes. These patterns can be compared to the deviation from target in the iteration at hand. If the deviation follows a typical pattern that was attributed to random scatter in the past, it is not compensated, while a pattern that diverges from typical scatter patterns is compensated. To achieve this goal the structural similarity index (SSI), which was originally introduced to calculate the similarity of pixel-based images by Wang et al. (2004), was adapted in this article to work with unstructured point clouds as can be extracted from the meshes at hand. The adapted similarity index in Eq. 6 compares nodal deviations for two point clouds and calculates an index with elements between 0 and 1 for each node:

$$\begin{aligned} &p_{SSI}\left(w_x, w_y\right) \\ &= 1 - \left(\frac{2\mu_x\mu_y + c_1}{\mu_x^2 + \mu_y^2 + c_1} \right)^{c_2} \left(\frac{2\sigma_x\sigma_y + c_1}{\sigma_x^2 + \sigma_y^2 + c_1} \right)^{c_3} \\ &\left(\frac{\sigma_{xy} + c_1}{\sigma_x\sigma_y + c_1} \right)^{c_4} \forall \text{ nodes}, \end{aligned} \tag{6}$$

where μ_x, μ_y, σ_x, σ_y, and σ_{xy} are the elementwise means, standard deviations, and cross-covariance for two deviation vectors $\boldsymbol{w}_i$ of meshes x and y.All values are calculated spatially with respect to a ball with radius r. All nodes within

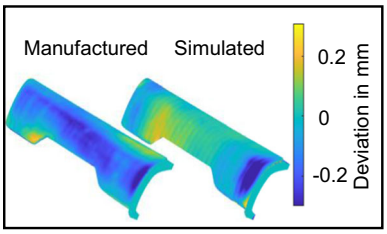

Fig. 2 Comparison of an exemplary manufactured component and the respective simulation

this ball are considered for the calculation. This enables the algorithm to deal with unstructured 3D point-clouds instead of 2D pixel data. c_1 is a constant, which is necessary for numerical stability. c_2 to c_4 are exponents, which weight the three terms to each other. This adapted SSI is able to calculate the local similarity of two meshes which have an identical connectivity. Equation 6 is used to compare the deviations $\boldsymbol{w}_i$ of recent iterations with past deviation patterns to evaluate their local similarity. If a local deviation pattern was associated with a random scatter in the past (e.g. caused by a fluctuation of the Young's modulus of the material), it will not be compensated, since a high similarity will result in a low p_{SSI}.

Process model

An FE model of the manufacturing process was implemented to test and tune several compensation strategies without the need to actually manufacture all components. The model was built with the simulation tool AscentAM, which was first described by Bayerlein (2020). The model consists of sequentially coupled FE calculations, which simulate the LPBF process by iteratively adding uniformly heated layers.

This simulation model of the LPBF process will be utilized to emulate typical batch fluctuations for a hybrid model of the production process without actually adapting the powder and manufacturing these parts. Figure 2 shows a comparison of the geometrical deviations due to the LPBF process compared to the target geometry. On the left side, an exemplary manufactured component is depicted, while the respective simulated component is shown on the right side.

The relative deformation pattern of the simulated and manufactured geometry is quite similar, while there is some offset in the absolute deformations. In the following, only relative deformation changes due to parameter variations are calculated with this simulation. This model can therefore be used to calculate the relative deformations of artificial batch variations without actually having to produce all the necessary iterations.

Based on this reference simulation, the material model was varied by increasing the material parameters Young's modulus (E), initial yield strength (IS) and thermal expansion (TE) individually by 10%. Furthermore, the process temperature (PT) was increased by 10%. The subsequent deviations from the reference simulation are shown in Fig. 3. These deviations from the reference calculation will be utilized as artificial deterministic batch fluctuations, resulting from different material batches in the hybrid model of an exemplary production cycle.

Hybrid model of a production cycle

Both approaches for the separation of scatter and deterministic deviations will be analysed in the following with respect to an exemplary production cycle of 80 manufacturing jobs or iterations. In order to save time and resources, a hybrid model of the production process is created to emulate realistic production results without having to manufacture 80 iterations for each compensation strategy. In this article, hybrid model describes the combined usage of simulated and experimentally obtained data to generate realistic process deviations. For each iteration a process deviation vector d, which describes the deviation of the workpiece from the manufacturing geometry, is calculated elementwise according to:

$$d_{i+1} = d_1 + d_{\text{det}} + d_{\text{scatter}} \forall \text{ nodes}, \tag{7}$$

where d_1 is the average deviation from target geometry, which was experimentally obtained. d_{det} is one of the four simulated deviations from the reference simulation due to changes in the material model or the process parameters. These deterministic deviations are valid for multiple iterations. d_{scatter} is an experimentally obtained job to job scatter from the experiments. Out of the eight available scatter data sets, one is randomly chosen for each iteration in this exemplary production cycle and scaled randomly by a factor picked out of a normally distributed population with mean 1 and standard deviation of 15%. This approach offers the change to combine the strength of Finite Element tools in calculating deterministic properties with the advantage of data-based approaches in describing non-deterministic process properties.

Results and discussion

Amplification of scatter

The results of the performed Monte Carlo analysis are depicted in Fig. 4. The results confirm that an α of 1 leads to a potentially unstable behaviour for large sample sizes and a significantly increasing scatter in the production cycle. The error bars in the figure indicate minimum and maximum results within the number of reruns of the Monte Carlo anal-

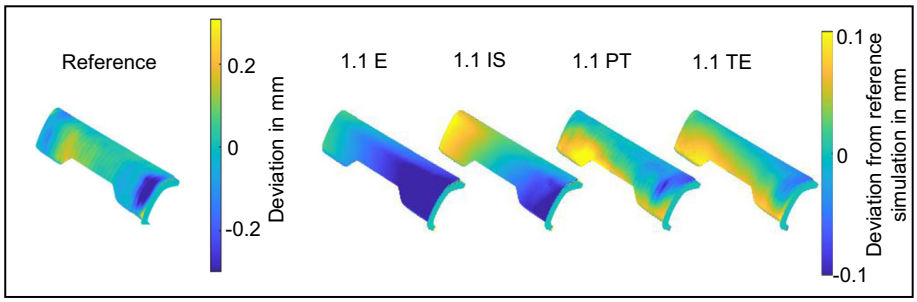

Fig. 3 Simulation results with artificially adapted material models to emulate batch fluctuations of the powder utilized for series production

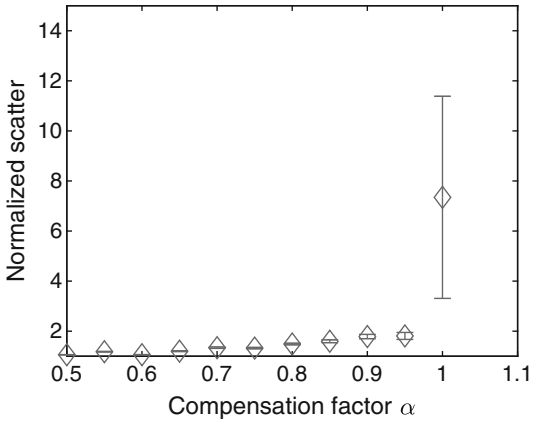

Fig. 4 Results of the Monte Carlo analysis of Eq. 1. The scatter in the produced geometry is amplified by the compensation

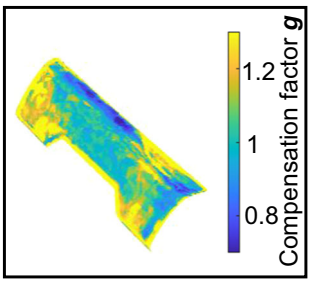

Fig. 5 Experimentally obtained local compensation factors g, which reflect the non-linear behaviour of the specific geometry at hand to linear compensation

ysis. This leads to the conclusion that it should be bounded below 1. For the geometry at hand, the standard deviation of the process compensation with Eq. 1 and an α of 0.95 leads approximately to $\sigma_{\text{compensated}} = 1.8\sigma_{\text{process}}$. For reference, for an α of 1.0 this factor averages to 7.3 for large sample sizes. Compensating for the statistical scatter with $\alpha \geq 1$ leads to an increasing and unstable oscillation of the geometry. This can be compared to a controller of a dynamic system with too much gain.

Quantification of non-linear behaviour

In order to quantify the non-linear effects of the compensation process, the 16 specimens which have been compensated two consecutive times according to Eq. 1 ($\alpha = 1$) are analysed regarding the resulting deviations in the next iteration. Therefore, the geometrical data of 32 compensated specimens are available for this calculation. In order to account for the non-linear behaviour, the compensation needs to be adjusted locally with a compensation factor $\boldsymbol{g}$ which is calculated elementwise using Eq. 8:

$$g = \frac{d_i}{d_i - d_{i+1}} \forall \text{ nodes} \tag{8}$$

Figure 5 shows $\boldsymbol{g}$ averaged over these 32 data sets. There are areas in this geometry, which react highly non-linear to the predeformation, which should be accounted for in future series compensation.

Local separation of scatter and deterministic deviations

In this section, three different compensation strategies are tested with the production cycle of 80 iterations described in Sect. 2.6. Figure 6 shows the experimentally obtained random scatter and the artificial deterministic batch fluctuations, which have been calculated with the FE model. All absolute deviations of all nodes on the functional area of the specimen have been averaged to provide one scalar to compare the different approaches and iterations. Furthermore, the deviations from target are shown for selected iterations for all three approaches. All four artificial deterministic deviations have similar amplitudes compared to the scatter, which shows the importance and difficulty to separate the two for the geometrical compensation. Over all the 80 iterations, both local compensation methods offer significant advantages over a constant $\boldsymbol{p\alpha} = 0.95$ (as determined in Sect. 3.1), which leads to an average deviation from target of 0.057 mm for each node. This value is calculated as a mean deviation over all nodes and iterations. The statistical approach (Eq. 5) reduces this by 13% to 0.049 mm, while the structural pattern analysis approach (Eq. 6) reduces it to 0.048 mm. Because the random scatter and the first iteration after a new batch with

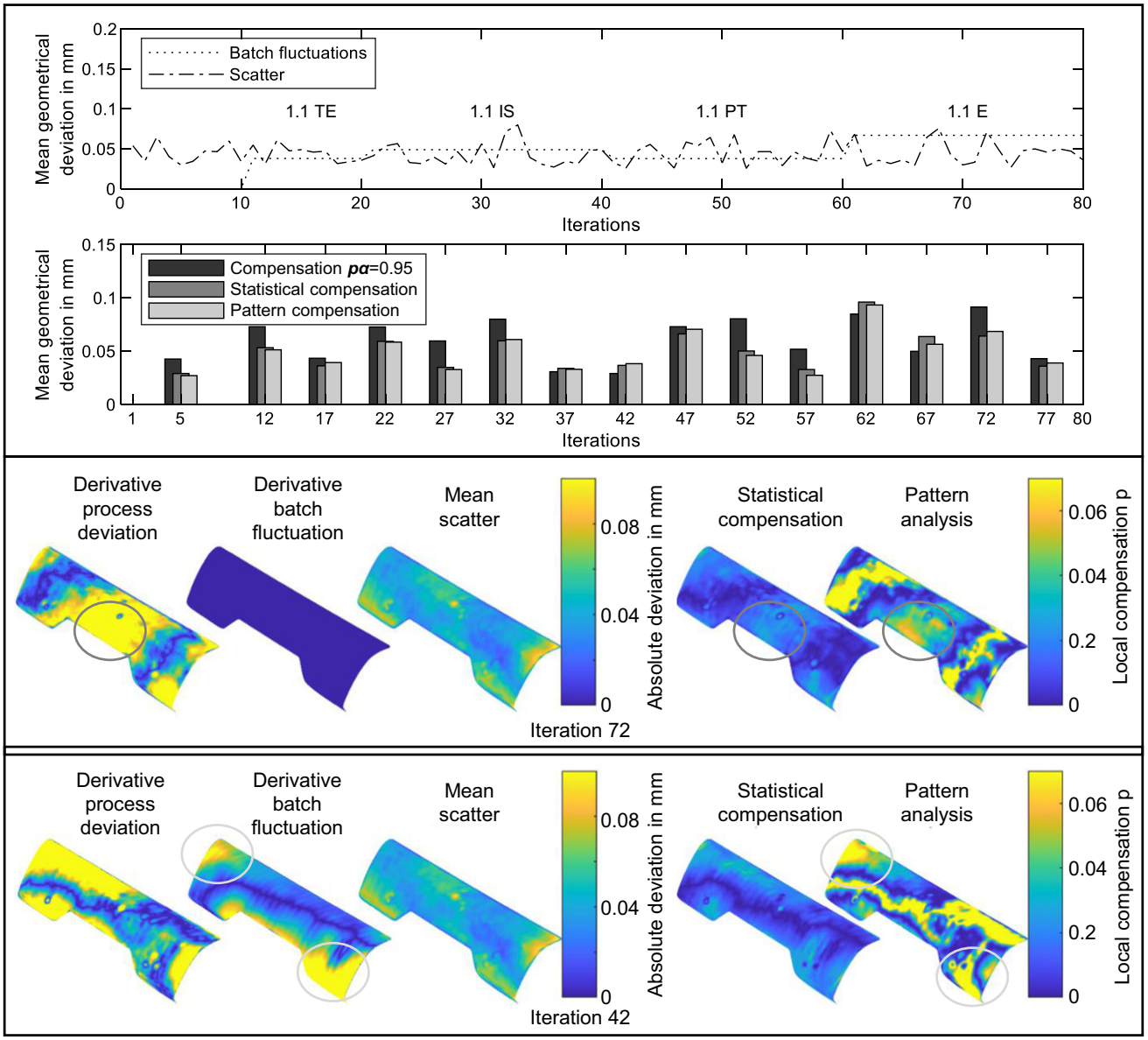

Fig. 6 Simulation results with artificially adapted material models to emulate batch fluctuations of the powder utilized for series production

deterministic deviations cannot be compensated, the minimum error, which is achievable in case of a perfect separation of scatter and deterministic deviations, is 0.045 mm. For reference: An uncompensated production cycle results in 0.083 mm average deviation. In order to discuss the consequences of the locally adapted compensation, iterations 42 and 72 are detailed in Fig. 4 middle and bottom. This includes the job to job change of the process deviation $\boldsymbol{d}$. Furthermore, the derivative of the batch fluctuation for the iteration at hand is shown and the mean experimental scatter, which is utilized for the two local approaches to calculate the local compensation factor $\boldsymbol{p}$. Iteration 72 is an example why both local compensations lead to better overall results. There is no change to the deterministic form deviations due to batch fluctuations. However, the scatter leads to changed process deviations. By comparing the process deviations to the scatter the compensation is scaled back and the error is reduced. Furthermore, it shows one advantage of the statistical compensation. If the scatter does not coincide well with the known scatter patterns (marked in dark gray), the statistical analysis is more robust, while the pattern analysis copes better with known deviation patterns. Iteration 42 is one of the few examples, where both algorithms lead to an increased mean geometrical error compared to a $\boldsymbol{p\alpha} = 0.95$. Both approaches lead generally to reduced compensation. Therefore, in case of a significant change in deterministic deviations, these are not fully compensated in the first iteration possible. Instead, it is gradually compensated over

multiple iterations. In this case, the pattern analysis algorithm has advantages over the statistical approach, since it compensates deterministic deviations well, which do not coincide with typical scatter deformation patterns (marked in light grey), independent of the absolute value. In contrast, the statistical approach scales the compensation back without the physical knowledge which can be gained by a posteriori analysing past iterations regarding their deformation patterns. Compared to the state of the art, these methods offer the opportunity to separate statistical scatter from deterministic deviations in an LPBF series production environment, which, to the best of the authors' knowledge, has not yet been investigated.

Conclusion

In this article, an approach was proposed for a geometrical deviation compensation in a LPBF series production. This approach accounts for time dependent deterministic form deviations due to, for example, batch fluctuations. Furthermore, the influence of random scatter on the compensation has been analysed and two equations have been proposed to handle the separation of scatter and deterministic form deviations. This is especially important for additive manufacturing processes with a high scatter compared to usual component tolerances. These methods will be adapted to other additive processes like binder jetting in the future which are suitable for series production as well. Furthermore, the compensation of time-dependent deterministic gemetrical deviations (e.g., an aging laser system) will be analysed.

Acknowledgements The authors would like to thank BMW Group for their cooperation. Furthermore, they would like to thank Tobias Grünn for his valuable input.

Author Contributions Conceptualization: PL; Methodology: CH, PL; Formal analysis: PL, CH; Data curation: PL, AH; Writing—original draft preparation: PL; Writing—review and editing: CH, AH; Software Resources: DW.

Funding Open Access funding enabled and organized by Projekt DEAL. The Federal Ministry of Education and Research of Germany (BMBF) funded this research under Grant Number: 13N15085.

Declarations

Conflict of interest The authors have no relevant financial or non-financial interests to disclose.

Data availability The datasets generated and analyzed during the current study are not publicly available due the fact that they constitute an excerpt of research in progress but are available from the corresponding author on reasonable request.

References

Akhavan, J., Lyu, J., & Manoochehri, S. (2023). A deep learning solution for real-time quality assessment and control in additive manufacturing using point cloud data. *Journal of Intelligent Manufacturing*. https://doi.org/10.1007/s10845-023-02121-4

Amor, S. B., Zongo, F., Louhichi, B., Tahan, A. & Brailovski, V. (2022). Dimensional deviation prediction model based on scale and material concentration effects for LPBF process. In *2022 International Additive Manufacturing Conference*. American Society of Mechanical Engineers, https://doi.org/10.1115/iam2022-93969.

Bayerlein, F. (2020). Managing form deviations in laser beam melting by pre-deformation. *Dissertation*.

Bourell, D., Kruth, J. P., Leu, M., Levy, G., Rosen, D., Beese, A. M., & Clare, A. (2017). Materials for additive manufacturing. *CIRP Annals, 66*(2), 659–681. https://doi.org/10.1016/j.cirp.2017.05.009

Cao, L., Li, J., Hu, J., Liu, H., Wu, Y., & Zhou, Q. (2021). Optimization of surface roughness and dimensional accuracy in LPBF additive manufacturing. *Optics & Laser Technology, 142*(3), 107246. https://doi.org/10.1016/j.optlastec.2021.107246

Ding, J., Qu, S., Zhang, L., Wang, M. Y., & Song, X. (2022). Geometric deviation and compensation for thin-walled shell lattice structures fabricated by high precision laser powder bed fusion. *Additive Manufacturing, 58*(103), 061. https://doi.org/10.1016/j.addma.2022.103061

Hartmann, C., Lechner, P., Himmel, B., Krieger, Y., Lueth, T. C., & Volk, W. (2019). Compensation for geometrical deviations in additive manufacturing. *Technologies, 7*(4), 83. https://doi.org/10.3390/technologies7040083

Li, C., Guo, Y., Fang, X., & Fang, F. (2018). A scalable predictive model and validation for residual stress and distortion in selective laser melting. *CIRP Annals, 67*(1), 249–252. https://doi.org/10.1016/j.cirp.2018.04.105

Luan, H., Grasso, M., Colosimo, B. M., & Huang, Q. (2019). Prescriptive data-analytical modeling of laser powder bed fusion processes for accuracy improvement. *Journal of Manufacturing Science and Engineering, 141*(1), 315. https://doi.org/10.1115/1.4041709

Schmidt, M., Merklein, M., Bourell, D., Dimitrov, D., Hausotte, T., Wegener, K., Overmeyer, L., Vollertsen, F., & Levy, G. N. (2017). Laser based additive manufacturing in industry and academia. *CIRP Annals, 66*(2), 561–583. https://doi.org/10.1016/j.cirp.2017.05.011

Vasileska, E., Demir, A. G., Colosimo, B. M., & Previtali, B. (2022). A novel paradigm for feedback control in LPBF: Layer-wise correction for overhang structures. *Advances in Manufacturing, 10*(2), 326–344. https://doi.org/10.1007/s40436-021-00379-6

Wang, Z., Bovik, A. C., Sheikh, H. R., & Simoncelli, E. P. (2004). Image quality assessment: From error visibility to structural similarity.

IEEE Transactions on Image Processing, 13(4), 600–612. https://doi.org/10.1109/TIP.2003.819861

Zhang, L., Zhu, H., Zhang, S., Wang, G., & Zeng, X. (2019). Fabricating high dimensional accuracy LPBFed ti6al4v part by using bi-parameter method. *Optics & Laser Technology, 117*, 79–86. https://doi.org/10.1016/j.optlastec.2019.04.009

Zhang, Y., & Yan, W. (2022). Applications of machine learning in metal powder-bed fusion in-process monitoring and control: Status and challenges. *Journal of Intelligent Manufacturing, 34*(6), 2557–2580. https://doi.org/10.1007/s10845-022-01972-7

Zongo, F., Simoneau, C., Timercan, A., Tahan, A., & Brailovski, V. (2020). Geometric deviations of laser powder bed-fused AlSi10mg components: Numerical predictions versus experimental measurements. *The International Journal of Advanced Manufacturing Technology, 107*(3–4), 1411–1436. https://doi.org/10.1007/s00170-020-04987-7